13th ewtec 2019 Proceedings of the 13th European Wave and Tidal Energy Conference 1-6 Sept 2019, Naples, Italy

Surface hydrodynamics of the Alderney Race from HF radar measurements

Guiomar Lopez, Anne-Claire Bennis, Yves Barbin, Laurent Benoit, Remi Cambra, Daniel C. Conley, Louis Marié, Alexei Sentchev, and Lucy R. Wyatt

***Abstract*—A pair of HF radars has been installed on the north-west coast of France to characterize the temporal and spatial variability of surface dynamics at the highly energetic Alderney Race. Radar measurements collected at two different transmitting frequencies are evaluated by comparison against in situ and modelled data. Agreement between the radar and in situ measurements, quantified by a Pearson correlation of 0.96, and 21 cm s^{-1} RMSE is deemed satisfactory. When compared to the modelled data, the agreement varies depending both on the radar transmitting frequency, and the location within the measuring grid. The highest differences are found in the area of strongest currents, where the radar-measured current magnitudes are generally lower. The latter is represented by a bias that can reach 0.8 m s^{-1}. On the same area, and throughout a 3-day period of exceptionally high tidal ranges, not only the radar and model current magnitudes differ, but also the flow asymmetry calculated with each of the two datasets does. Whereas the radar measurements show a positive flow asymmetry, with higher velocities measured at the peak of the flood, the analysis of the modelled data resulted in the opposite outcome.**

***Index Terms*—Alderney Race, HF radar, waves, surface current.**

I. Introduction

SITES with high tidal stream potential are often located in coastal environments where the interaction between numerous physical processes results in complex hydrodynamics. Consequently, an accurate quantification of the tidal stream energy requires at the very least, an understanding of not only the current itself, but the wave field and the interactions between the two [1], [2]. In addition, the appropriate characterisation of the resource, as well as the optimisation of site siting requires an understanding of the spatial variability of the tidal current [3].

With their ability to provide a spatial snapshot of the surface current as well as the wave field with a good compromise between temporal and spatial resolution, HF radars can represent an efficient tool for the characterisation of tidal resources when used along with in situ devices and numerical models. With this aim, a pair of HF radars has been recently installed at the Contentin peninsula, in the north-west coast of France to monitor the Alderney Race, a tidal current flowing between Cap de La Hague (France) and the island of Alderney (UK), which due to the constraints exerted by the aforementioned land boundaries is amongst the strongest tidal currents in Europe.

HF radars transmit an electromagnetic (EM) signal at a frequency within the HF band (3-30 MHz), and record the backscatter that results from its interaction with the sea surface. Spectral analysis of this backscatter results in what is known as the Doppler spectrum, which is characterized by two prominent peaks resulting from the coherent backscatter of the EM signal off first-order linear waves of half the transmitted wavelength, travelling toward or away the radar stations. The position of these peaks, known as first-order or Bragg peaks, allows resolving for the speed of the current, as well as its direction if the data from the two radars are combined. In addition, higher order waves with half the radio wavelength may also contribute to the measured signal, appearing on the sides of the first-order peaks mentioned above. This part of the spectrum, commonly referred to as the second-order energy, can be used to retrieve the directional spectrum of waves (e.g. [4], [5], [6]) or some of its summary parameters (e.g. [7], [8]).

Since they are deployed at the coastline, HF radars are not directly subjected to the marine conditions in the same way in situ devices are, and this constitutes a clear advantage in harsh environments like the Alderney Race. Nonetheless, given the complexity and the extreme oceanographic conditions that can occur in the area, challenges to the technique and the processing algorithms still arise.

This study shows the first results derived from the measurements of the Alderney Race HF radar. By comparing the results against in situ measurements and modelled results, we expect to identify the factors affecting their quality to be able to design specific treatments for their improvement. The paper is organised as follows. In the next section we describe the study site

ID 1646 TRC. This work benefited from France Energies Marines and State financing managed by the National Research Agency under the Investments for the Future program bearing the reference ANR-10-IED-0006-07.

G. Lopez , A-C. Bennis and L. Benoit are at M2C (CNRS UMR 6143), Université de Caen, 14000 Caen, France (e-mails: guiomar.lopez-fernandez@unicaen.fr, acbennis@unicaen.fr, laurent.benoit@unicaen.fr).

Y. Barbin is an independent researcher retired from the Institut Méditerranéen d'Océanologie (MIO) (CNRS/Aix-Marseille Université/IRD/Université du Sud Toulon-Var), 83041 Toulon, France (email: barbin.yves@orange.fr)

R. Cambra is at France Energies Marines (FEM), 29280 Plouzane, France (e-mail: Remi.Cambra@france-energies-marines.org).

D. C. Conley is at the School of Biological and Marine Sciences, Plymouth University, Plymouth PL4 8AA, UK (e-mail: daniel.conley@plymouth.ac.uk).

L. Marié is at Laboratoire d'Oceanographie Physique et Spatiale (LOPS), IFREMER, 29280 Plouzane, France (e-mail: Louis.Marie@ifremer.fr)

A. Sentchev is at Laboratoire d'Océanologie et de Géosciences (CNRS UMR 8187), Université du Littoral - Côte d'Opale, 62930 Wimereux, France (e-mail: alexei.sentchev@univ-littoral.fr)

L. R. Wyatt is at the School of Mathematics and Statistics (SoMaS), Sheffield University, Sheffield S3 7RH, UK (e-mail: l.wyatt@sheffield.ac.uk)

and the data used here. In section III we summarise the methods used to process the data. In section IV we present the results, which are discussed in section V.

II. Materials and Methods

The Alderney Race refers to the current flowing through the strait located between Cap de La Hague, in the north-west coast of France, and the Island of Alderney (UK). The site is characterised by a mean spring tidal range between 6 and 10 m, water depths between 25 and 65 m, and current speeds that can reach the 5 m s^{-1} as a result of the flow acceleration between Cap de La Hague and the Channel Islands. The prevailing wind directions are between the south-west and west, and can exceed the 16 m s^{-1} more than half of the time during winter [9], giving rise to quite energetic wind seas. In addition, although to some extend shielded by Alderney, the area is also exposed to the Atlantic swell, which is an important component of the wave climate at the Alderney Race.

A. HFR data

A pair of WERA phased-array radars [10] has been installed on the north-west coast of France to monitor the surface current and waves of the Alderney Race. The individual stations are located at Jobourg and Goury, approximately 5 km apart (Fig. 1). Each site has two square 4-element transmitting arrays, which operate at 13.5 MHz and 24.5 MHz, respectively, and a 16-element receiving array shared by the two transmitting frequencies.

Data used for this work were collected during two days of a neap tide at the end of January 2018, and 5 days covering a spring tide at the beginning of October 2018. The first dataset extends through the 24 and 25 January 2018, and was chosen to coincide with a period when ADCP measurements were simultaneously available. With the exception of the first hours of the 25 January, when the Goury radar operated at 24.5 MHz, both radars transmitted at 13.5 MHz. At the latter frequency, radars acquired measurements during 17 min 45 s, every 30 minutes at approximately 1.5 km range resolution and 14° azimuthal resolution. The second dataset spans 5 days of a spring tide and was collected alternating the two available frequencies. Measurements at 13.5 MHz were collected twice per hour during 17 min 45 s each time, and recorded to files of coherent data that were stored every 128 samples (about 33 s). These data were later combined to obtain time series of approximately 8 min length. Transmission at 24.5 MHz was also performed twice per hour, during 8 min 52 s each time. Similarly to the low transmitting frequency, data were stored every 33 s, and then combined to ∼8 min time series. Range and azimuthal resolution at 13.5 MHz are the same as in the first period, while the range and azimuthal resolutions at 24.5 MHz are 750 m and 7°, respectively. As for the depth of the measurements, it is well accepted that HF radar samples the current velocity integrated over a depth that depends on the transmitted frequency [11]. Such depth is about 88 cm at 13.5 MHz, and 48 cm for the 24.5 MHz. Finally, in all cases data were set onto a regular grid at 0.5 km spacing (Fig. 1).

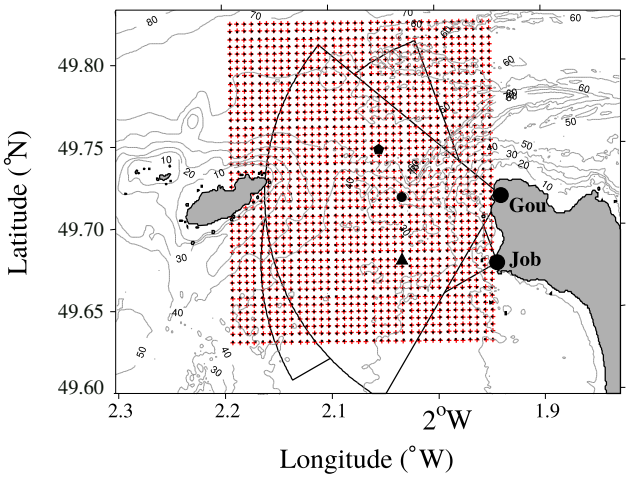

Fig. 1. Map showing the radar stations at Goury (Gou), and Jobourg (Job), their maximum coverage for wave measurement (black arcs), and measuring grid (black dots). The model grid points used for comparison are shown with red crosses. The black triangle indicates the position where the ADCP was deployed. The black pentagon and circle show two grid points that will be commented further in the text.

The radial data acquired by each of the two stations were posteriorly combined to produce surface current vectors over the measurement grid. Radar directional ocean wave spectra were derived from the recorded backscatter using the Seaview algorithm [12], which solves the equations that describe the second-order scatter from ocean waves [13]. The result is a wave number directional spectrum with a variable amount of wave numbers, and 30 directions at 12° resolution. This was subsequently converted into the directional frequency spectra using the wave dispersion relation.

B. ADCP

The ADCP data used in this work were collected with a bottom-mounted 500 kHz Teledyne RDI Sentinel V50 that was deployed within the radar's coverage area from 15 October 2017 to 9 July 2018 at about 37 m depth (Fig. 1). The instrument recorded current velocities every 5 minutes in bursts of 1 minute at 1 Hz, with a vertical resolution of 1 m [14]. Waves were sampled during 20 min at 2 Hz, every hour. Raw measurements were processed using RDI's software in order to obtain current velocities over the water column. Because the data are intended for comparison against the radar's measurement of the surface current, only the uppermost bin was kept for further analysis. However, bins located close to the surface are affected by sidelobe reflection and wave contamination, hence the first 30% of the water column below the surface level determined by the ADCP's surface track was discarded, and only data from the bin directly underneath were used for subsequent analysis. The average depth of this bin was 25 m, approximately 10 m below the surface. These data were further averaged to match the radar's 30 min time resolution.

The ADCP orbital velocities were processed into directional spectra using RDI's software. The iterative maximum likelihood method (IMLM; [15]) was applied to compute directional spectra at 0.0156 Hz frequency resolution, and 90 directions at 5° resolution.

C. Hydrodynamic model

The three-dimensional hydrodynamic model MARS 3D [16], coupled to the spectral wave model WAVEWATCH-III [17] was used to compute the flow over a grid covering the radar's field of view, with a spatial resolution of 120 m. Selected points, which were the closest to a radar grid point were kept for the comparisons hereby presented (Fig. 1). MARS 3D solves the hydrostatic primitive equations under the Boussinesq assumption and following the terrain coordinate. WAVEWATCH III computes the propagation of ocean waves by solving the wave action conservation equation. Wave forcing is taken into account in the coastal ocean model via the vortex force method ([18], [19], [20]) allowing to reproduce wave effects on the entire water column (e.g. Stokes drift effects, enhancement of the bottom friction, changes in vertical mixing). The coupled model has been largely validated for nearshore cases in the past ([21], [22] and recently for the Alderney Race [23]. Exchanges are two-way and occur every 20 seconds: MARS 3D sends surface velocities and sea surface height to WAVEWATCH III, which then sends the wave forcing terms to MARS 3D. The surface-most level from the water column modelled with MARS 3D was selected for comparison against the radar's results.

D. Methods

Comparisons between radar, ADCP and model were performed calculating basic descriptive statistics. Namely, the Pearson correlation coefficient, the root-mean-squared-error (RMSE) and the difference between the means of pairs of datasets (bias) were calculated. In addition to the comparison against ADCP measurements and modelled results, the radar surface currents were used to describe the general hydrodynamics of the Alderney Race. For that, we calculated the mean current over the measurement grid, and the current flow characteristics in terms of tidal ellipses. The parameters that determine the latter were obtained applying a principal component analysis to the radar current vectors. Finally, the tidal flow asymmetry was calculated as the ratio between the mean flood and ebb velocities ($\bar{v}_{flood}/\bar{v}_{ebb}$) at each grid point.

III. Results

E. Alderney Race hydrodynamics

The radar dataset collected in October 2018 is used here to study the general circulation during a spring tide at the Alderney Race. The tidal ellipses shown in Fig. 2 suggest a tidal flow that arrives from the South and bends towards the NE as a response to the bathymetry. The ellipses resulting from the analysis of the two radar frequencies are similar, although

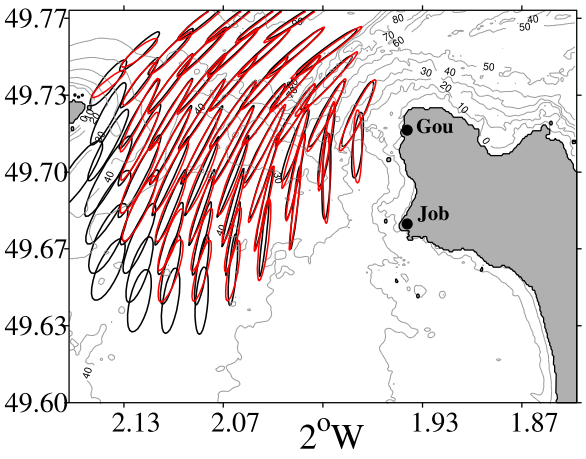

Fig. 2. Tidal ellipses calculated from the currents vectors measured at 13.5 MHz (black) and 24.5 MHz (red).

the results obtained at 24.5 MHz indicate a slightly higher current magnitude measured at that frequency, especially in the region of maximum current velocity, approximately in front of Goury. The eccentricity of the ellipses, defined as the quotient between their major and minor axes, is maximal at the middle of the strait, where the current flows backwards and forwards, and increases near the coast and at the southern part of the grid, where the behaviour is closer to a vector rotating about a point.

The time averaged current magnitude measured over the 3-day period of maximum tidal ranges is shown in Fig. 3. Both frequencies show significant spatial variations on the surface current velocity, which attains its maximum values at the NE corner of the field of view and across the strait, over the 30 m isobath. The values of average current velocities range between 1.4 and 2.6 m s^{-1} and are generally higher at 24.5 MHz, especially in the areas where the current reaches its maximum values. There, the results obtained at 24.5 MHz are on average 20 cm s^{-1} higher than those measured at 13 MHz.

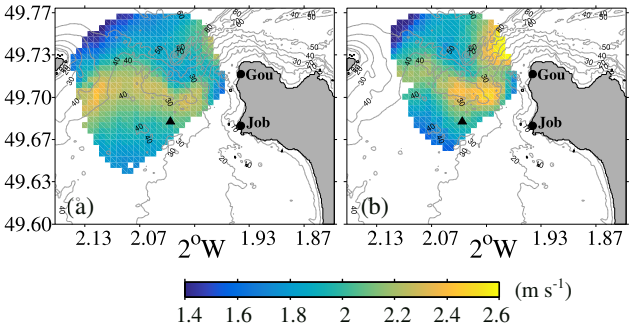

Fig. 3. Mean current magnitude (m s^{-1}) measured between 8 and 11 October 2018 at (a) 13.5 MHz and (b) 24.5 MHz.

F. Radar - ADCP comparisons

Radar surface velocities collected between 24 and 25 January 2018 are hereby compared against the ADCP velocity time series extracted from the first usable bin

below the surface. The dataset covers one half tidal cycle characterized by a tidal range of about 4 m, and a surface current that exceeded the 2 m s^{-1} around high tide. Over this period the wind was blowing from the south-west, with speeds between 8 and 10 m s^{-1}. The comparison of the current magnitude revealed a good agreement between the two devices, represented by Pearson correlation coefficient of 0.96, 21 cm s^{-1} RMSE, and a slight positive bias that indicates the radar velocities are on average 6 cm s^{-1} higher that the ADCP's. As shown in Fig. 4, the highest differences appear at the times of maximum velocity, when the radar-derived current velocity surpasses that of the ADCP. Regarding the direction of the flow, the highest discrepancies between methods appear around slack tide, when the tide is turning. The ADCP measurements indicate that the current veers towards the NE later than the radar measurement, whereas the turn towards the opposite direction seems to occur at the same time in both datasets. On average, the radar-derived directions differ in about 17° from the ADCP's.

Comparison of the radar's wave results obtained during the same two days analysed above were presented in [24]. The results at and around slack tide showed radar wave spectra that were accurate both in shape and energy content, as compared to the ADCP results. This was translated into wave height differences between 3 and 16 cm. On the other hand, during high tide the radar overestimated the energy density, showing a difference of about 2 m^2Hz^{-1} at the spectral peak compared to the ADCP. Similarly to the quality, the spatial extent of the results was reduced during the times of maximum current.

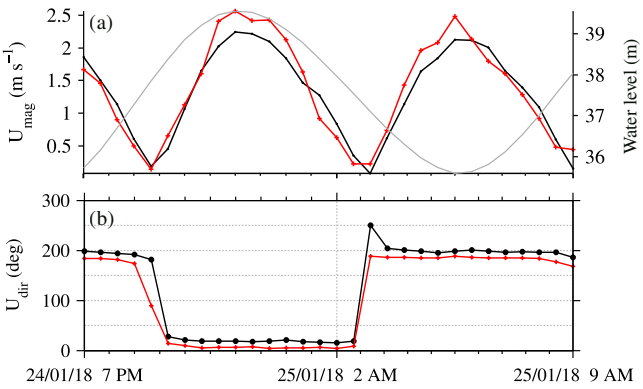

Fig. 4. Time series of (a) ADCP (black) and radar surface velocities (red), and (b) ADCP (black) and radar (red) current direction. The latter follows the oceanographic convention, that is the direction to which the currents are going, measured clockwise from North.

G. Radar - MARS 3D comparisons

The radar's spatial measurements collected from 5 to 11 October 2018 were compared to the outputs of the model described in Section II. During the first part of the studied period (from 6 to 7 October) a strong wind was blowing from the North, reaching the 20 m s^{-1} on the night of 6 October. The wind then turned west, and its speed fell to an average 3 m s^{-1} during 8 to 10 October, to then start turning toward the East, increasing again until reaching 9 m s^{-1} on the 11 October. Following the wind, waves propagated from the North during 6 and 7 October, reaching a significant wave height of 2 m $^{-1}$ on the night of 6 October. Accordingly, they then veered west and decreased to significant wave heights below 1 m.

During this period, the highest discrepancies between model and radar mean spring current magnitude (Fig. 5) are concentrated over the area of maximum velocities shown in Fig. 3 for both radar frequencies. However, the maximum difference between the model and the radar's 24.5 MHz measurements was 20 cm s^{-1} lower than that obtained for the 13.5 MHz comparison.

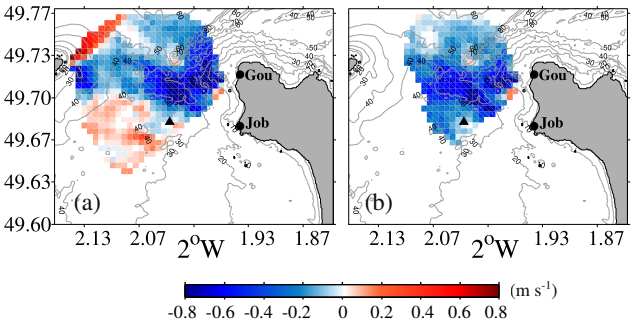

Fig. 5. Bias between radar and model surface current magnitudes over the period 8 to 11 October 2018 at (a) 13.5 MHz, and (b) 24.5 MHz.

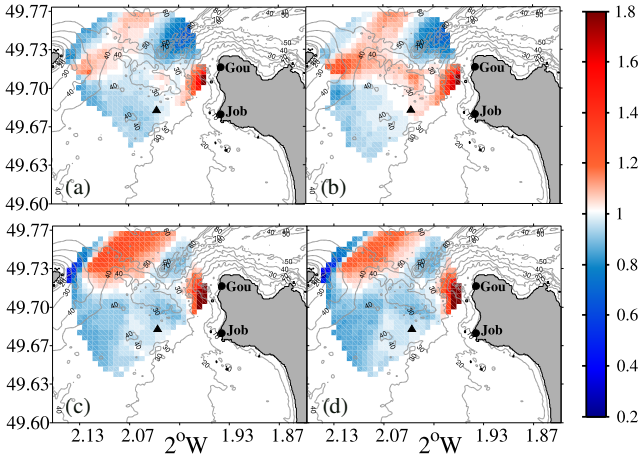

Fig. 6. Current velocity asymmetry calculated from radar measurements at 13.5 MHz (upper panels) and modelled results (lower panels) collected between (a, c) 5 and 7 October 2018, (b, d) 8 and 11 October 2018. Colour scale indicates the ratio between flood and ebb velocities. A ratio greater than one means the flood current is stronger than the ebb, and vice versa.

Fig. 6 shows the ratio between the current magnitude during the rising and falling phases of the tide, calculated for two periods with an average difference of 2 m in tidal range. A ratio greater than one means the flood current is stronger than the ebb, and vice versa. During the period of lower tidal range, and with the exception of a strip in the north-western part of the radar's coverage, both radar and model show an overall dominance of the ebb velocities over the study area. On the other hand, throughout the three days when the tidal range reaches its maximum values

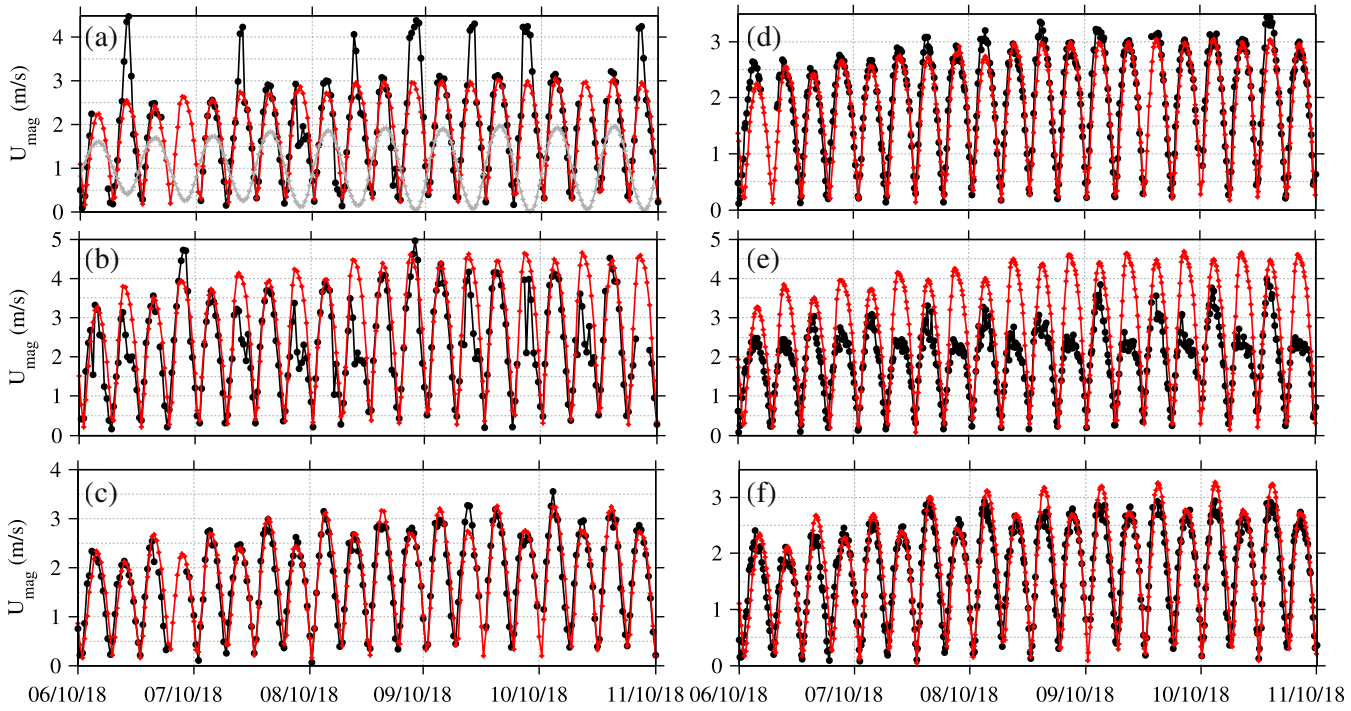

Fig. 7. Surface current velocity computed with MARS 3D (red), and radar-measured (black) at 24.5 MHz (a - c), and 13.5 MHz (d - f). For each frequency, measurements at three grid points are shown, (a, d) is the ADCP position shown in Fig.1, (b, e) 49.71°N, 2.03°W and (c, f) 49.75°N, 2.05°W. The last two grid points are shown in Fig. 1 with an black circle and pentagon, respectively. The grey line in panel (a) is the water level (not at scale).

(up to 9 m at some parts of the field of view), the radar flow asymmetry shows flood dominance across a diagonal line connecting the Jobourg headland with the island of Alderney. This is the opposite to what was obtained with the modelled data, whose flow asymmetry values remain similar during the two studied periods. The asymmetry calculated with the 24.5 MHz measurements (not shown) follows the same pattern than the 13.5 MHz results shown in Fig.6.

The differences between model and radar current magnitudes during flood and ebb suggested by the above-discussed flow asymmetry values can be clearly seen in Fig. 7. Time series obtained at three different grid points are shown. At the northern-most point (Fig. 7 c and f), radar and model current magnitudes are in good agreement, both showing lower peak velocities during ebb than flood. On the other hand, at a point located at the boundary between a region of 30 m depth to the south, and the deep region known as La Hague deep toward the north, the differences between radar and model increase, especially at the time of ebb peak magnitude, when the radar current velocity is well below the modelled result. In addition, while the differences between radar and model are observed for both radar frequencies, the lowest magnitudes are attained by the 13.5 MHz radar measurements, which are lower than both the model and the 24.5 MHz radar results over the studied period. Finally, at the location where the ADCP had been deployed the comparison between model and radar measurements at 13.5 MHz gives similar results to the ADCP-radar comparison shown in Fig. 4, namely, a good agreement between measurements, with slightly higher values measured by the radar at the times of maximum current velocity. The 24.5 MHz comparison alternates between a very good agreement with the model magnitudes and big overestimations during low-water.

IV. Discussion

The radar measurements collected during the end of January 2018 compared well with the ADCP measurements. With an average current magnitude of 1.31 m s^{-1} measured by the acoustic device, the 21 cm s^{-1} RMS difference between the latter and the radar can probably be attributed to the measurement techniques themselves, which differ in their sampling volume, as well as in the depth of their measurements in the water column.

Comparison against modelled results yielded a maximum bias of 0.8 m s^{-1} across the area where the maximum current magnitudes are attained. Otherwise, the bias was found to be around 0.2 m s^{-1} over the rest of the coverage area. The most striking feature of the observed differences between radar and model is the opposite flow asymmetry found over the region of maximum current velocities and during two days of exceptionally high tidal ranges. While the radar's flow asymmetry resulted in flood dominance during the period of highest tidal ranges, the model showed ebb dominance during the whole period covered by the dataset collected during October 2018. With no other in situ measurements to verify this finding, it is difficult to know whether it is the radar or the model which is not accurately capturing the current magnitude during ebb in this area. Given the number of tidal constituents and the 500 m resolution bathymetry included in the model,

we expect it to be able to reproduce an asymmetry inversion such as that observed on the radar results during the period of high tidal ranges. However, given the abrupt change in the topography, there is always certain degree of smoothing. This might result in an underestimation of the effect exerted by this bathymetric step on the flow during low water. On the other hand, the surface current at this site reaches values exceeding the maximum radial velocity that can be accurately measured with HF radars operating at the frequencies transmitted by our systems, which is 4.16 m s^{-1} at 13.5 MHz, and 3.13 m s^{-1} at 24.5 MHz. Errors derived from this limitation could explain the lower current velocities measured by the radar as compared to the model in the area where the maximum current velocities are attained. However, the results obtained at the lower frequency, which has a higher velocity threshold, are generally smaller than those collected at 24.5 MHz. Hence, this limitation does not appear to be the source of the differences found. The lower spatial resolution of the 13.5 MHz measurements can, however, explain the lower results obtained at this frequency as compared to the 24.5 MHz measurements and the model results. Taking the grid point of Fig. 7 (b, e), located in the area of maximum current velocity about 7 km away from the radar sites, the sea patch affecting the measurements at 24.5 MHz is approximately 0.85 x 1.5 km after window weighting, while the 13.5 MHz measurements represent an integration of the scatter off waves present in a 1.5 x 3 km sea patch. At this location, close to an edge where the sea floor topography varies abruptly from 30 to 80 m, the Bragg waves reflecting the radar signal within the aforementioned sea patch can be under the influence of non-uniform sheared current fields. This results in the broadening of the measured radar Doppler spectra [25], which no longer have a clear distinctive peak (used to calculate current velocity), and this may be the source of the lower measured values.

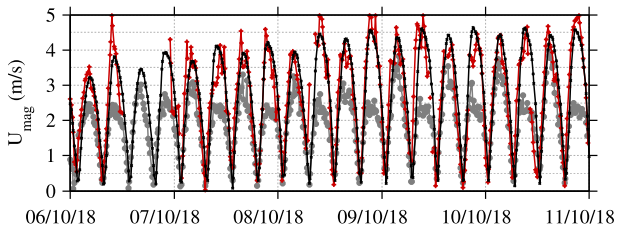

Fig. 8. Surface current velocity computed with MARS 3D (black), and radar-measured at 13.5 MHz and calculated with the beam-forming technique (grey), and the direction finding technique (red). The time series corresponds to the grid point at 49.71°N, 2.03°W (black circle in Fig. 1).

In order to verify whether the relatively coarse resolution is the source of these differences, the radar raw data are currently being reprocessed using the Multiple Signal Classification (MUSIC) direction finding algorithm (see [26] for further details). The results obtained at the same grid point discussed above are shown in Fig. 8, and indicate that higher velocities can be achieved when the radar signals are processed with this method. However, the fine tuning essential to ensure the best performance of the algorithm is a work in progress. Thus, these results must be regarded with caution. Hence, although more research is needed to understand the discrepancies found between radar measurements and modelled currents, it is clear that the former bring the opportunity to question and verify the modelled spatial outputs, otherwise difficult to validate in complex areas such as the Alderney Race, where long-term spatial measurements are scarce.

ACKNOWLEDGEMENT

The authors would like to thank Lucille Furgerot and the crew of the CNRS research vessels "Thalia" and "Côtes de la Manche" for their involvement in the deployment and posterior processing of the ADCP data used for this paper.

REFERENCES

[1] A. G. Davies, M. J. Lewis, P. E. Robins, S. P. Neill, and M. R. Hashemi, "Effect of waves on the tidal energy resource at a planned tidal streamarray," *Renewable Energy*, vol. 75, pp. 626–639, 2014. [Online]. Available: http://dx.doi.org/10.1016/j.renene.2014.10.029

[2] M. J. Lewis, S. P. Neill, M. R. Hashemi, and M. Reza, "Realistic wave conditions and their influence on quantifying the tidal stream energy resource," *Applied Energy*, vol. 136, pp. 495–508, 2014. [Online]. Available: http://dx.doi.org/10.1016/j.apenergy.2014.09.061

[3] P. E. Robins, S. P. Neill, M. J. Lewis, and S. L. Ward, "Characterising the spatial and temporal variability of the tidal-stream energy resource over the northwest European shelf seas," *Applied Energy*, vol. 147, pp. 510–522, 2015. [Online]. Available: http://dx.doi.org/10.1016/j.apenergy.2015.03.045

[4] J. J. Green and L. R. Wyatt, "Row-action inversion of the Barrick-Weber equations," *Journal of Atmospheric and Oceanic Technology*, vol. 23, no. 3, pp. 501–510, 2006.

[5] Y. Hisaki, "Nonlinear inversion of the integral equation to estimate ocean wave spectra from HF radar," *Radio Science*, vol. 31, no. 1, pp. 25–39, 1996.

[6] N. Hashimoto and M. Tokuda, "A Bayesian Approach for Estimation of Directional Wave Spectra with HF Radar," *Coastal Engineering Journal*, vol. 41, no. 2, pp. 137–149, 2003.

[7] K. W. Gurgel, H. H. Essen, and T. Schlick, "An empirical method to derive ocean waves from second-order bragg scattering: Prospects and limitations," *IEEE Journal of Oceanic Engineering*, vol. 31, no. 4, pp. 804–811, 2006.

[8] D. E. Barrick, "Extraction of wave parameters from HF radar," *Radio Science*, vol. 12, pp. 415–423, 1977.

[9] O. Planchon, "A study of the coastal climates in France using temperature and precipitation data (1961-1990)," *Meteorological Applications*, vol. 7, no. 3, pp. 217–228, 2000.

[10] K. W. Gurgel, H. H. Essen, and S. P. Kingsley, "High-frequency radars: Physical limitations and recent developments," *Coastal Engineering*, vol. 37, no. 3-4, pp. 201–218, 1999.

[11] R. H. Stewart, "INSTRUMENTS AND METHODS HF radio measurements of surface currents," *Current*, vol. 21, pp. 1039–1049, 1974.

[12] L. R. Wyatt, "High-Frequency Radar Measurements of the Ocean Wave-Directional Spectrum," *IEEE Journal of Oceanic Engineering*, vol. 16, no. 1, pp. 163–169, 1991.

[13] D. E. Barrick and B. L. Weber, "On the Nonlinear Theory for Gravity Waves on the Ocean's Surface. Part II: Interpretation and Applications," *Journal of Physical Oceanography*, vol. 7, no. 1, pp. 11–21, 2002.

[14] L. Furgerot, P. B. Du Bois, Y. Méar, M. Morillon, E. Poizot, and A. C. Bennis, "Velocity profile variability at a tidal-stream energy site (Alderney Race, France): From short (second) to yearly time scales," in *2018 OCEANS - MTS/IEEE Kobe Techno-Oceans, OCEANS - Kobe 2018*. IEEE, 2018, pp. 1–8.

[15] H. E. Krogstad, "Maximum likelihood estimation of ocean wave spectra from general arrays of wave gauges," *Modeling, Identification and Control*, vol. 9, no. 2, pp. 81–97, 1988.

[16] P. Lazure and F. Dumas, "Lazure, Dumas_2008_An external-internal mode coupling for a 3D hydrodynamical model for applications at regional scale (MARS).pdf," *Advances in Water Resources*, vol. 31, pp. 233–250, 2008.
[17] Y. A. Twumasi and E. C. Merem, "GIS and remote sensing applications in the assessment of change within a coastal environment in the niger delta region of Nigeria," Tech. Rep. 1, 2006.
[18] F. Ardhuin, N. Rascle, and K. A. Belibassakis, "Explicit wave-averaged primitive equations using a generalized Lagrangian mean," *Ocean Modelling*, vol. 20, no. 1, pp. 35–60, 2008.
[19] A. C. Bennis, F. Ardhuin, and F. Dumas, "On the coupling of wave and three-dimensional circulation models: Choice of theoretical framework, practical implementation and adiabatic tests," *Ocean Modelling*, vol. 40, no. 3-4, pp. 260–272, 2011.
[20] J. C. McWilliams, J. M. Restrepo, and E. M. Lane, "An asymptotic theory for the interaction of waves and currents in coastal waters," *Journal of Fluid Mechanics*, vol. 511, pp. 135–178, 2004.
[21] A. C. Bennis, F. Dumas, F. Ardhuin, and B. Blanke, "Mixing parameterization: Impacts on rip currents and wave set-up," *Ocean Engineering*, vol. 84, pp. 213–227, 2014.
[22] A. C. Bennis, F. Dumas, and B. Blanke, "Modulation of wave-current interactions by horizontal mixing and spatial resolution," *Ocean Modelling*, vol. 99, pp. 75–85, 2016.
[23] A. C. Bennis, P. B. Du Bois, F. Dumas, C. Lathuillère, F. Adong, and J. F. Filipot, "Towards a realistic numerical modelling of wave-current-turbulence interactions in alderney race," in *2018 OCEANS - MTS/IEEE Kobe Techno-Oceans, OCEANS - Kobe 2018*. IEEE, 2018, pp. 1–7.
[24] G. Lopez, A.-C. Bennis, Y. Barbin, L. Benoit, R. Cambra, D. C. Conley, T. Helzel, and J. Lagarde, "Hydrodynamics of the Alderney Race : HF Radar Wave Measurements," in *Proceedings of the 7th International Conference on Ocean Energy, ICOE*. Cherbourg: OES, 2018, pp. 1–6. [Online]. Available: https://www.icoe-conference.com/publication/hydrodynamics-of-the-alderney-race-hf-radar-wave-measurements/
[25] M. L. Heron, "Line broadening on HF ocean surface radar backscatter spectra," *IEEE J. Ocean. Eng.*, vol. 10, no. 4, 1985.
[26] A. Sentchev, P. Forget, Y. Barbin, and M. Yaremchuk, "Surface circulation in the Iroise Sea (W. Brittany) from high resolution HF radar mapping," *Journal of Marine Systems*, vol. 109-110, no. SUPPL., pp. S153–S168, 2013. [Online]. Available: http://dx.doi.org/10.1016/j.jmarsys.2011.11.024